HHS Public Access

Author manuscript

Bone. Author manuscript; available in PMC 2020 April 01.

Published in final edited form as:

Bone. 2019 April ; 121: 172–180. doi:10.1016/j.bone.2019.01.016.

Defective Circadian Control in Mesenchymal Cells Reduces Adult Bone Mass in Mice by Promoting Osteoclast Function

Kelly Tsang, BA[1], **Haoming Liu, MS**[1], **Yen Yang**[2], **Julia F. Charles, MD/PhD**[1,3], **Joerg Ermann, MD**[1,3,*]

[1]Division of Rheumatology, Immunology and Allergy, Brigham and Women's Hospital, Boston, MA 02115, USA

[2]Division of Rheumatology, University of Massachusetts, Worcester, MA 01655, USA

[3]Harvard Medical School, Boston, MA 02115, USA

Abstract

Serum bone turnover markers show diurnal variation in humans, suggesting that circadian rhythms contribute to normal bone physiology. This conclusion is corroborated by bone phenotypes in mice with genetic disruption of the circadian molecular clock mechanism, for instance via deletion of the transcription factor Brain and Muscle Arntl-like 1 (*Bmal1*). To dissect the contribution of circadian molecular clocks in individual bone cell types, we generated mice with conditional deletion of *Bmal1* in osteoclasts (*Ctsk-cre*) and in mesenchymal cells of the limbs (*Prx1-cre*). We report that deletion of *Bmal1* in osteoclasts had no effect on trabecular or cortical bone parameters *in vivo* or on osteoclast differentiation *in vitro.* In contrast, $Bmal1^{f/f}$.*Prx1-cre* mice had significantly less trabecular and cortical bone than $Bmal1^{f/f}$ littermate controls, recapitulating the bone phenotype of *Bmal1* germline deficient mice. The number of osteoblast precursors in the bone marrow of $Bmal1^{f/f}$.*Prx1-cre* mice was similar to wild-type controls, while the *in vitro* differentiation capacity of *Bmal1*-deficient osteoblast precursors, measured as induction of alkaline phosphatase activity, was significantly lower. Despite this, serum procollagen type 1 N-terminal propeptide (P1NP), a measure of bone formation *in vivo,* was higher in $Bmal1^{f/f}$.*Prx1-cre* mice than in $Bmal1^{f/f}$ mice. Consistent with a high bone turnover state in the mutant mice, the bone resorption marker serum C-terminal telopeptides of Type I collagen (CTX-I) was also elevated, and $Bmal1^{f/f}$.*Prx1-cre* mice had a higher number of tartrate resistant acid phosphatase (TRAP) positive osteoclasts than $Bmal1^{f/f}$ controls. These results demonstrate that adult bone mass in mice is controlled by the intrinsic circadian molecular clock in mesenchymal cells but not

[*]corresponding author: Joerg Ermann, MD, Division of Rheumatology, Immunology and Allergy, Brigham and Women's Hospital, HBTM Room 6002P, 60 Fenwood Road, Boston, MA 02115, USA, jermann@bwh.harvard.edu, phone: 617-525-1227, fax: 617-525-1010.

Authors' roles:

Study design: JE and JFC. Study conduct: KT, HL, YY, JFC, and JE. Data collection: KT, HL, YY, JFC, and JE. Data analysis: KT, JFC, and JE. Drafting Manuscript: JE. Revising manuscript and content: JE and JFC. Approving final version of manuscript: KT, HL, YY, JFC, and JE. JE takes responsibility for the integrity of the data analysis.

osteoclasts. The effect of the mesenchymal cell clock on bone turnover appears to involve osteoblast-osteoclast cross-talk.

Keywords

Genetic animal models; bone; osteoclasts; osteoblasts; transcription factors; microCT

1. Introduction

Many biological processes follow circadian rhythms which, in humans and other mammals, are generated by cell-intrinsic molecular clocks that generate diurnal changes in gene expression, affecting about 10 % of the transcriptome in any given cell type [1]. At the molecular level, the mammalian molecular clock is a transcriptional-translational feedback mechanism. Positive regulators (Bmal1, Clock, Npas2) drive the expression of negative feedback regulators (Per and Cry genes, Nr1d1), which in turn inhibit the expression and activity of the positive regulators in a cycle that lasts approximately 24 hours [2]. A central clock in the hypothalamus receives sensory input from the eyes and communicates with peripheral tissues via neuronal and hormonal pathways to synchronize peripheral tissue clocks with the environment. Disruption of the synchrony between environmental and endogenous circadian rhythms, for instance in shift workers, or dysfunction of the molecular clock mechanism in older people, has been linked to disease. Understanding the molecular mechanisms underlying circadian control may also be important for optimal drug therapy [3].

Several serum bone turnover markers in humans show diurnal variation [4], suggesting a role for circadian molecular clocks in bone physiology. This conclusion is corroborated by bone phenotypes in mice with genetic disruption of the circadian molecular clock mechanism. Mice with germline deletion of *Cry1/Cry2* or *Per1/Per2,* transcription factors that form the negative feedback loop of the circadian molecular clock, were shown to have a high bone mass phenotype thought to be mediated via effects of leptin and the sympathetic nervous system on osteoblast function [5]. Bmal1 is the major positive regulator of the molecular clock. Published bone phenotypes for mice with germline deletion of *Bmal1* have varied, reporting either low bone mass [6] or no bone phenotype [5, 7]. We found that *Bmal1* germline mutant mice have a low bone mass phenotype. To further clarify the role of circadian molecular clocks in bone physiology we generated mice with conditional deletion of *Bmal1* in osteoclasts and mesenchymal cells, respectively. Our results confirm a critical function for circadian molecular clocks in mesenchymal cells, as conditional deletion of *Bmal1* in mesenchymal cells but not in osteoclasts recapitulated the low bone mass phenotype seen in germline *Bmal1* deficient mice. Moreover, our data suggest that the development of low bone mass in these mice is the result of increased bone turnover and involves cross-talk between osteoblasts and osteoclast lineage cells.

2. Material and Methods

2.1 Mice

Bmal1$^{f/f}$ mice (B6.129S4(Cg)-Arntl^{tm1Weit}/J) [8], *Prx1-cre* mice (B6.Cg-Tg(Prrx1-cre)1Cjt/J)[9] and *ROSA26*$^{mT/mG}$ mice (B6.129(Cg)-Gt(ROSA)26Sor$^{tm4(ACTB-tdTomato,-EGFP)Luo}$/J) [10], all on a C57BL/6 background, were purchased from the Jackson Laboratory. *Ctsk-cre* mice [11] were a gift of Shigeaki Kato, University of Tokyo, Japan and have been backcrossed to C57BL/6 for 20 generations. The *Bmal1*$^{-}$ allele arose by Cre-mediated germline deletion in offspring of a female *Bmal1*$^{f/f}$*.Prx1-cre* mouse [9]. *Bmal1*$^{-/-}$ mice are infertile [7]. *Bmal1*$^{-/-}$ and *Bmal1*$^{+/+}$ littermates were generated by crossing *Bmal1*$^{+/-}$ parents. *Bmal1*$^{f/f}$*.Ctsk-cre, Bmal1*$^{f/+}$*.Ctsk-cre,* and *Bmal1*$^{f/f}$ littermates were generated by mating *Bmal1*$^{f/+}$*.Ctsk-cre* and *Bmal1*$^{f/f}$ parents. *Bmal1*$^{f/f}$*.Prx1-cre* and *Bmal1*$^{f/f}$ controls were derived by mating *Bmal1*$^{f/f}$*.Prx1-cre males* with *Bmal1*$^{f/f}$ females. Age and sex of the mice included in each experiment are specified in the text. In most cases, 8-week-old male knockout mice and control littermates were pooled from multiple litters for analysis. Consecutive animals were analyzed without selection. Mice were housed in microisolator cages with up to 5 mice per cage in specific pathogen-free animal facilities at the Harvard T.H. Chan School of Public Health or at Brigham and Women's Hospital under standard 12 hour light - 12 hour dark conditions, the beginning of the light period corresponding to circadian time (CT) 0 hours. Animals had access to standard mouse chow (PicoLab Mouse Diet 20, #5058, LabDiet) and water ad libitum. All studies were performed according to institutional and NIH guidelines for care and use of laboratory animals and were approved by the Institutional Animal Care and Use Committees of Harvard Medical School and Brigham and Women's Hospital.

2.2 Micro-computed tomography

A Scanco Medical μCT 35 system with an isotropic voxel size of 7 μm was used for micro-computed tomographic (microCT) analysis of femurs. All microCT analysis was performed blinded to the genotype of the analyzed mice. Bones were scanned in 70% ethanol using an X-ray tube potential of 55 kVp, an X-ray intensity of 0.145 mA and an integration time of 600 ms. A region beginning approximately 0.28 mm proximal to the growth plate and extending 1.1 mm proximally was selected for trabecular bone analysis. A second region 0.6 mm in length centered at the midpoint of the femur was used to measure cortical bone parameters. A semi-automated contouring approach was used to distinguish cortical and trabecular bone. The region of interest was thresholded using a manually determined global threshold set at 368 mg HA/cm^3 for trabecular bone and 708 mg HA/cm^3 for cortical bone. 3-D microstructural properties of bone, including bone volume fraction (BV/TV), trabecular number (Tb N), trabecular thickness (Tb Th), trabecular separation (Tb Sp), trabecular bone mineral density (Tb BMD), cortical thickness (Cort Th), and cortical bone mineral density (Cort BMD) were calculated using software supplied by the manufacturer.

2.3 Histology

For osteoclast quantification, femurs from 8-week-old *Bmal1*$^{f/f}$ and *Bmal1*$^{f/f}$*.Prx1-cre* mice were fixed in 10% neutral buffered formalin (NBF) for 24 hours followed by decalcification with 14% EDTA for 14 days and paraffin embedding. 5 μm sections were stained for TRAP

activity [12] and counterstained with hematoxylin. The OsteoMeasure Analysis System (OsteoMetrics) was used to determine the osteoclast surface per bone surface within a region of interest 100 μm proximal to the growth plate. Two sections from each of 6 mice per group were analyzed. Slides were imaged on a Leica DM2000 LED microscope. For deletion analysis, femurs from 4-week-old *Bmal1*$^{f/f}$*.ROSA26*$^{mT/mG}$ and *Bmal1*$^{f/f}$*.Ctsk-cre.ROSA26*$^{mT/mG}$ mice were fixed in 4% paraformaldehyde (PFA) and decalcified with 14% EDTA for 2 days. Cryosections (16 μm) were stained with DAPI and imaged with a Leica TCS SP8 confocal microscope.

2.4 *In vitro* osteoclast assays

Total bone marrow cells were cultured on suspension dishes (Corning) in α-MEM with ribonucleosides (Corning) supplemented with 10% fetal bovine serum (FBS), 100 U/ml penicillin G, 1 mg/ml streptomycin (both Cellgro), and 40 ng/ml macrophage colony-stimulating factor (M-CSF, R&D). After 3 days, non-adherent cells were replated at a density of $6x10^4$ cells/well in 24 well plates or $1x10^4$ cells/well in 96 well plates and cultured in medium with 10 ng/ml RANKL (R&D) and 20 ng/ml M-CSF for 5-7 days. Osteoclasts were then stained for TRAP activity or harvested for quantitative polymerase chain reaction (qPCR). For reporter analysis, *Bmal1*$^{f/f}$*.Ctsk-cre.ROSA26*$^{mT/mG}$ and *Bmal1*$^{f/f}$*.ROSA26*$^{mT/mG}$ control osteoclasts were grown on 1 mm glass coverslips (Sigma) coated in FBS, fixed in 4% PFA and stained with DAPI. An Olympus FSX100 Inverted Microscope was used to evaluate EGFP expression.

2.5 *In vitro* osteoblast assays

Long bones were isolated from 7-10 day old mice, crushed and digested with 2 mg/ml dispase II (Roche) and 1 mg/ml collagenase type II (Worthington Biochemicals) in α-MEM for 30 minutes at 37 °C with agitation, whereupon the supernatant was collected (Fraction 1) and replaced with fresh digestion medium. Two subsequent digestions were performed identically (Fraction 2, 3). For colony forming unit (CFU) assays, Fraction 1 was plated at 1.5×10^5 cells/well in medium onto 6 wells plates, expanded for 4 days and then differentiated for 21 days in α-MEM medium without ribonucleosides (Corning) supplemented with 10 % FBS, 100 U/ml penicillin G, 1 mg/ml streptomycin, 50 μg/ml ascorbic acid and 5 mM β-glycerophosphate. Cultures were fixed in 10% neutral buffered formalin (NBF) and stained for alkaline phosphatase activity. Colonies were counted by two independent investigators blinded to genotype. Fraction 2 and 3 were pooled, plated onto 10 cm dishes and passaged every other day for 10 days. The expanded population was then plated at 1.1×10^4 cells/cm^2, differentiated for 28 days as described and stained with alizarin red and von Kossa. Cultures were also stained and analyzed for alkaline phosphatase activity as described [13]. The alkaline phosphatase index (AP index) was derived by normalizing alkaline phosphatase activity to Alamar Blue (Invitrogen) fluorescence as a measure of cell viability. All cultures were performed with cells from individual mice.

2.6 Quantification of *Bmal1* deletion

Genomic DNA was extracted from primary osteoclast or osteoblast cultures using a standard protocol for tail DNA isolation, i.e. digestion with proteinase K (Sigma) followed by isopropanol precipitation. Real-time quantitative PCR analysis of DNA samples was done on

a StepOnePlus Real-Time PCR System (Applied Biosystems) with Fast SYBR Green Master Mix (Applied Biosystems) and the following primer pairs: FL5 - GCTCACAGGCTGCAGAGG, TTCCAGACGACCAGGTTTGG; *D3Mit319* - TCTCCCTCACTTTTTCCTTCC, AACAGCCAGTCCAGCAAATC; *D7Mit97* - CTTCCACACATCCACACTTACA, TCTTGGTCTCCAGCCTCTGT. The FL5 primer pair flanks the upstream *loxP* site in the floxed *Bmal1* locus yielding a PCR product of ~170 base pairs (bp). Cre-mediated excision of the floxed DNA segment abrogates the reverse primer site and results in loss of the PCR product. The satellite markers *D3Mit319* and *D7Mit97* were used for quantification of total DNA, with the primers above yielding PCR products of 197 bp and 138 bp, respectively, for C57BL/6 genomic DNA. Abundance of the floxed *Bmal1* allele was measured by normalizing the cT value for FL5 over the mean cT value for *D3Mit319* and *D7Mit97* using the ΔcT method. Data were further normalized by dividing each individual data point by the mean of the $Bmal1^{f/f}$ samples in a given experiment.

2.7 Gene expression in cortical bone

Diaphyseal bone from femurs was flushed to remove the marrow. RNA was isolated from the remaining cortical bone with Trizol reagent (Life Technologies) using a bullet blender (Next Advance) to homogenize the tissue. 500 ng of RNA was used to generate cDNA (Affinity Script RT-PCR cDNA Synthesis Kit, Agilent Technology). Real-time quantitative PCR (qPCR) was performed in duplicate using Sybr green reagent (Life Technologies). Primer sequences were *Opg* – TGTCCAGATGGGTTCTTCTCA, CGTTGTCATGTGTTGCATTTCC; *Rankl* – CAGCATCGCTCTGTTCCTGTA, CTGCGTTTTCATGGAGTCTCA; Hprt – GTTAAGCAGTACAGCCCCAAA, AGGGCATATCCAACAACAAAC.

2.8 Serum bone turnover markers

Blood was collected from mice by cardiac puncture following euthanasia at the time points indicated in the text. Serum was isolated using serum separator tubes (BD Biosciences) and analyzed using commercial ELISA kits for CTX-I and P1NP (IDS), or RANKL and OPG (R&D).

2.9 Statistical Analysis

Statistical analysis and graphing were done with Prism 7 (Graphpad Software). Two experimental groups were compared using the Student's *t* test and three groups by one-way ANOVA. The bars in all graphs represent mean and standard deviation (SD).

3. Results

3.1 Adult *Bmal1* germline knockout mice have a low bone mass phenotype

We analyzed femurs from 8-week-old male mice with germline deletion of *Bmal1* ($Bmal1^{-/-}$) by microCT. This age was selected for analysis to avoid confounding of the results by the progressive arthropathy in $Bmal1^{-/-}$ mice [7], which might restrict mobility at later time points. At 8 weeks of age, the trabecular bone mass in male $Bmal1^{-/-}$ mice was about 40% lower than in $Bmal1^{+/+}$ male littermates (Fig. 1A). Corresponding changes were observed for trabecular number, thickness and separation. Trabecular BMD was reduced by

5% (Fig. 1B). *Bmal1*$^{-/-}$ mice also showed a slight but statistically significant reduction of cortical thickness and cortical BMD (Fig. 1C and D).

3.2 Osteoclast-specific deletion of Bmal1 has no effect on microCT bone parameters

To address whether the reduction in trabecular bone mass is a function of *Bmal1* deficiency in osteoclast or osteoblasts, we generated mice with conditional deletion of *Bmal1* using a mouse strain with a floxed *Bmal1* allele [8] that has been widely used to analyze the effects of tissue-specific *Bmal1* deletion. In this strain, Cre recombinase activity excises the exon encoding the helix-loop-helix domain of *Bmal1* resulting in a functional null mutant [8]. First, we generated mice with osteoclast-specific deletion of *Bmal1* using the *Ctsk-cre* driver strain [11] comparing 8-week-old *Bmal1*$^{f/f}$.*Ctsk-cre* mice with *Bmal1*$^{f/+}$.*Ctsk-cre* littermates. None of the standard trabecular or cortical bone microCT parameters demonstrated a trend in the direction of the phenotype observed in *Bmal1* germline mutants (Fig. 2A and B, Fig. S1).

We had chosen this experimental setup to avoid potential *Cathepsin K* gene-dosage effects caused by the *Ctsk-cre* knock-in allele. Subsequent experiments revealed that there was no significant difference in microCT parameters between male *Ctsk-cre* positive mice and wild-type C57BL/6 littermates at 8 weeks (Fig. S2), and we confirmed that *Bmal1* haploinsufficiency does not result in a discernable bone phenotype (Fig. S3). We thus concluded that *Bmal1* deficiency in osteoclasts has no effect on bone. However, contrary to our findings, a recent report suggested that mice with osteoclast-specific *Bmal1* deletion have higher bone mass than *Bmal1*$^{f/f}$ mice at 12 weeks of age [14]. To address this discrepancy, we performed an additional *in vivo* study. *Bmal1*$^{f/+}$.*Ctsk-cre* mice were crossed with *Bmal1*$^{f/f}$ mice to generate littermates with the three genotypes *Bmal1*$^{f/f}$, *Bmal1*$^{f/+}$.*Ctsk-cre* and *Bmal1*$^{f/f}$.*Ctsk-cre*, which were analyzed at 12 weeks (Fig. 2C-F). Again, there were no statistically significant differences between male *Bmal1*$^{f/f}$.*Ctsk-cre* mice and littermate controls (Fig. 2C-F) confirming our initial observation.

We verified that *Ctsk-cre* was functional in our mice by crossing the *ROSA*$^{mT/mG}$ reporter allele into the *Bmal1*$^{f/f}$.*Ctsk-cre* line. Analysis of 4-week-old *Bmal1*$^{f/f}$.*Ctsk-cre*.*ROSA*$^{mT/mG}$ mice demonstrated green fluorescence near the growth plate in an osteoclast-like distribution (Fig. 3A). No statistically significant difference in osteoclast differentiation from the bone marrow of *Bmal1*$^{f/f}$.*Ctsk-cre* vs. *Bmal1*$^{f/f}$ bone marrow was observed *in vitro* (Fig. 3B), despite documented osteoclast Cre-activity demonstrated using the *ROSA*$^{mT/mG}$ reporter (Fig. 3C) and RANKL-induced *Bmal1* deletion measured by qPCR (Fig. 3D). This qPCR assay quantifies abundance of the floxed *Bmal1* allele using a primer pair flanking the upstream *loxP* site. Cre-mediated excision of the floxed gene segment removes the reverse primer binding site and results in loss of the PCR product (Fig. S4). In conclusion, the analysis of *Bmal1*$^{f/f}$.*Ctsk-cre* mice provided no evidence for an effect of osteoclast-specific deletion of *Bmal1* on bone parameters that would mimic the bone phenotype observed in mice with germline deletion of *Bmal1.*

3.3 Conditional deletion of *Bmal1* maps the bone phenotype to *Bmal1*-deficient mesenchymal cells

We then analyzed mice with Bmal1 deficiency in mesenchymal cells using the *Prx1-cre* driver [9]. In contrast to deletion in osteoclasts, mesenchymal cell-specific deletion of *Bmal1* in *Bmal1*$^{f/f}$*.Prx1-cre* mice lowered trabecular bone mass in 8-week-old mice with a reduction in BV/TV by ~20% relative to *Bmal1*$^{f/f}$ littermate controls (Fig. 4A, 4E and F). We observed corresponding statistically significant changes in trabecular number, thickness and separation. Trabecular BMD, cortical thickness and cortical BMD were also decreased (Fig. 4B-D), similar to germline *Bmal1* deletion. The same phenotype was present in 8-week-old female mice (Fig. S5). Real-time quantitative PCR data in Fig. S6 provide evidence for *Bmal1* deletion and disruption of the circadian molecular clock in the extremities of *Bmal1*$^{f/f}$*.Prx1-cre* mice. Bmal1 deficiency in mesenchymal cells thus recapitulates the bone phenotype observed in *Bmal1* germline-knockout mice, mapping the effect of Bmal1 deficiency on bone to a mesenchymal cell lineage derived from *Prx1-cre* positive precursors.

In order to study potential mechanisms, we compared the *in vitro* osteogenic potential of bone marrow cells from *Bmal1*$^{f/f}$ and *Bmal1*$^{f/f}$*.Prx1-cre* mice. There was no difference in the number of osteoblast precursors between the two genotypes (Fig. 5A and B). However, we observed a small but statistically significant reduction in osteogenic potential of *Bmal1*$^{f/f}$*.Prx1-cre* bone marrow stromal cell osteoblast precursors measured as induction of alkaline phosphatase activity under osteoblast differentiating conditions (Fig. 5C and D). Panel E in Fig. 5 demonstrates deletion of *Bmal1* in osteoblast cultures from *Bmal1*$^{f/f}$*.Prx1-cre* mice, whereas the *Bmal1*$^{f/f}$ locus is in germline configuration in DNA isolated from the tail, consistent with the *Prx1-cre* expression pattern [9].

3.4 Evidence for high bone turnover in *Bmal1*$^{f/f}$*.Prx1-cre* mice

We then analyzed bone turnover markers in the serum of *Bmal1*$^{f/f}$ and *Bmal1*$^{f/f}$*.Prx1-cre* mice every 6 hours over the course of one day. Contrary to our expectation, serum P1NP as a marker of bone formation was increased in *Bmal1*$^{f/f}$*.Prx1-cre* mice at all time points. Serum CTX-I as a marker of *in vivo* osteoclast activity was also increased (except at circadian time 6 hours). This suggests that the reduced bone mass in *Bmal1*$^{f/f}$*.Prx1-cre* mice is due to increased bone turnover compared with *Bmal1*$^{f/f}$ wild-type controls, resulting in an overall negative balance. Consistent with this interpretation we found a small but statistically significant increase in the number of osteoclasts in *Bmal1*$^{f/f}$*.Prx1-cre* mice (Fig. 6B). The *in vitro* osteoclastogenic potential of *Bmal1*$^{f/f}$ and *Bmal1*$^{f/f}$*.Prx1-cre* bone marrow did not differ (Fig. S7), suggesting that the effect of *Bmal1* deficiency on osteoclast numbers and resorption activity in *Bmal1*$^{f/f}$*.Prx1-cre* mice is the result of osteoblast-osteoclast cross-talk *in vivo.* Others have reported that Bmal1 controls the expression of RANKL in osteoblasts [15]. Consistent with this, we observed increased expression of *Rankl* in diaphyseal cortical bone of *Bmal1*$^{f/f}$*.Prx1-cre* mice (Fig. 6C). However, expression of *Opg* was also increased resulting in a decreased ratio of *Rankl/Opg* expression in bone (Fig. 6C). We then examined serum protein levels of RANKL and OPG over the course of the 24-hour day. At circadian time 6 hours, serum levels of RANKL in *Bmal1*$^{f/f}$*.Prx1-cre* mice were decreased relative to *Bmal1*$^{f/f}$ controls, with no significant difference in RANKL at other time points (Fig. 6D).

Serum OPG levels were indistinguishable between the two strains (Fig. 6D). Thus, increased local or systemic RANKL activity is unlikely to be the mechanism that explains how *Bmal1*-deficient osteoblasts promote bone resorption and high bone turnover. Instead, Bmal1 may control secondary pathways by which osteoblasts promote osteoclast formation or activity.

4. Discussion

The low bone mass phenotype we observed in *Bmal1*$^{-/-}$ and *Bmal1*$^{f/f}$*.Prx1-cre* mice mirrors reports of increased bone mass in mice with germline deletion of either *Per1/Per2* or *Cry1/Cry2* [5]. Bmal1 drives the expression of these transcription factors, which then oppose the activity of Bmal1 [16]. Deletion of *Bmal1* thus disrupts the molecular clock at a different point in the circadian cycle than deletion of *Per1/Per2* or *Cry1/Cry2.* This has been likened to the removal of either the thermostat or the furnace from a heating system [17] resulting in opposing changes in the expression of clock-controlled genes and, correspondingly, divergent phenotypic outcomes when either the clock driver *Bmal1* or the negative regulators *Per1/Per2* or *Cry1/Cry2* are deleted. We cannot rule out that Bmal1 has additional functions outside of its role as a core regulator of the circadian molecular clock. Nevertheless, our results identify mesenchymal cells as the driver of the bone phenotype in *Bmal1*$^{-/-}$ mice, with osteoclast-specific *Bmal1* deletion having no effect on bone mass, cortical thickness or BMD. Whether *Per1/Per2* or *Cry1/Cry2* deletion similarly acts through effects in mesenchymally derived cells remains to be shown.

Our results are consistent with those of Samsa et al., who demonstrated a low bone mass phenotype in *Bmal1*$^{-/-}$ mice compared with wild-type controls using microCT [6]. In contrast, Bunger et al., in their original description of *Bmal1*$^{-/-}$ mice [7] did not find a significant decrease in areal bone mineral density in *Bmal1*$^{-/-}$ mice using Piximus densitometry, although there was a trend toward decreased femoral bone mineral density. Our results also contrast with those of Xu et al. who reported an osteoclast-intrinsic role for Bmal1 in controlling bone mass [14]. Possible explanations for these diverging results include differences in sensitivity of microCT compared to densitometry, genetic background of the knockout mice, stringency of using littermate controls, and possibly effects of local microbiota [18].

Studies of serum bone turnover markers in humans and mice have demonstrated robust circadian variations of osteoclast markers [19, 20]. Our data show that Bmal1 deficiency in the progeny of *Prx1* expressing cells results in a small increase in the number of osteoclasts. Additionally, it is likely that Bmal1 deficiency in mesenchymal cells affects osteoclast function *in vivo,* as the circadian curve of serum CTX-I in *Bmal1*$^{f/f}$*.Prx1-cre* mice is flattened compared with *Bmal1*$^{f/f}$ controls. The lack of a bone phenotype in mice with osteoclast-specific deletion of *Bmal1* suggests that circadian osteoclast activity is mostly under extrinsic control by non-osteoclast clocks. These data suggest that osteocytes, osteoblasts or other mesenchymally derived cells regulate osteoclast activity over the course of a 24-hour day. It has been reported that Bmal1 directly controls the expression of RANKL in osteoblasts [15], and we found increased *Rankl* expression in cortical bone from *Bmal1*$^{f/f}$*.Prx1-cre* mice. However, we also measured increased *Opg* expression with a decreased *Rankl/Opg* ratio in *Bmal1*$^{f/f}$*.Prx1-cre* mice compared to *Bmal1*$^{f/f}$ animals.

Furthermore, serum RANKL levels in *Bmal1*$^{f/f}$*.Prx1-cre* mice were not elevated compared with wild-type littermate controls, at least at 8 weeks of age. How the circadian molecular clock in mesenchymal cells impacts the number and/or function of osteoclasts thus remains to be determined.

Although osteoblast differentiation from *Bmal1*$^{f/f}$*.Prx1-cre* precursors was modestly decreased *in vitro,* serum markers of bone formation were actually higher in *Bmal1*$^{f/f}$*.Prx1-cre* mice. This is consistent with the findings of Fu et al., who reported that 8-week-old *Bmal1*$^{-/-}$ mice had an increased bone formation rate but also accelerated bone resorption, as demonstrated by increased urine deoxypyridinoline levels in their study [5]. Similarly, bone resorption activity as measured by serum CTX-I was higher in*Bmal1*$^{f/f}$*.Prx1-cre* mice during the majority of the circadian cycle. Taken together, our data suggest that the low bone mass in *Bmal1*$^{f/f}$*.Prx1-cre* mice is due to increased bone turnover. Although we do not have dynamic histomorphometry data, we hypothesize that Bmal1 deficiency in mesenchymal cells results in increased bone resorption mediated by wild-type osteoclasts and secondary stimulation of bone formation. However, this increase in bone formation in *Bmal1*$^{f/f}$*.Prx1-cre* mice is not sufficient to fully compensate for the loss due to cell-intrinsic defects in Bmal1-deficient osteoblasts.

Limitations of our study include the typical issues encountered when analyzing conditional knockout mice. Gene deletion is an artificial disruption of cellular function, which may impact the translatability of such studies. Moreover, results are critically dependent on the deletion characteristics of the specific cre strains used including the potential for gene deletion in cells other than the targeted cell lineage. We also did not analyze the impact of disrupting environmental circadian rhythms on bone.

Interestingly, circadian disruption by shift work is associated with increased markers of bone resorption in women [21]. Furthermore, in a small study, nurses working rotating shifts were found to have lower BMD and a higher prevalence of osteopenia than day time workers in the same hospital [22]. The negative consequences of circadian disruption on bone health was confirmed in the Nurses' Health Study, where nurses working night shifts for 20 or more years had a relative fracture risk of 1.37 compared to nurses who had never worked shifts [23]. And in the Osteoporotic Fractures in Men (MrOS) study, there was a modest association of the daytime to nighttime activity ratio with areal BMD and change in areal BMD over 4 years [24]. Alternations in diurnal hormone patterns, particularly of reproductive hormones, have been proposed as the mechanism explaining the effect of circadian rhythm disruption on bone [21, 23]. Our work and that of others, using mouse models, demonstrate that mesenchymal cell-intrinsic circadian molecular clocks are major drivers of diurnal variation in bone turnover. Extrinsic circadian rhythm disruptions may affect bone health by interfering with physiological circadian osteoblast-osteoclast interactions.

Supplementary Material

Refer to Web version on PubMed Central for supplementary material.

Acknowledgements

We thank Jacobo Ramirez for excellent animal care.

This work was supported by NIH grants R03 AR066357 (JE) and K08 AR062590 (JFC), the Maldari Fund, the Bettina Looram Fund, and the Center for Skeletal Research Core (NIH P30 AR066261).

Abbreviations

Bmal1	Brain and Muscle Arntl-like 1
P1NP	Procollagen type 1 N-terminal Propeptide
CTX-I	C-terminal Telopeptides of Type I Collagen
TRAP	Tartrate Resistant Acid Phosphatase
Cry	Cryptochrome
Per	Period
CT	Circadian Time
microCT	micro-computed tomography
BV/TV	Bone Volume/Tissue Volume
Tb N	Trabecular Number
Tb Th	Trabecular Thickness
Tb Sp	Trabecular Separation
Tb BMD	Trabecular Bone Mineral Density
Cort Th	Cortical Thickness
Cort BMD	Cortical Bone Mineral Density
NBF	Neutral Buffered Formalin
RANKL	Receptor Activator of Nuclear factor Kappa-B Ligand
OPG	Osteoprotegerin
Ctsk	Cathepsin K
Prx1	Paired Related Homeobox 1

References

[1]. Zvonic S, Ptitsyn AA, Kilroy G, Wu X, Conrad SA, Scott LK, Guilak F, Pelled G, Gazit D, Gimble JM, Circadian oscillation of gene expression in murine calvarial bone, J Bone Miner Res 22(3) (2007) 357–65. [PubMed: 17144790]

[2]. Bass J, Takahashi JS, Circadian integration of metabolism and energetics, Science 330(6009) (2010) 1349–54. [PubMed: 21127246]

[3]. Kaur G, Phillips C, Wong K, Saini B, Timing is important in medication administration: a timely review of chronotherapy research, Int J Clin Pharm 35(3) (2013) 344–58. [PubMed: 23329340]

[4]. Joseph F, Chan BY, Durham BH, Ahmad AM, Vinjamuri S, Gallagher JA, Vora JP, Fraser WD, The circadian rhythm of osteoprotegerin and its association with parathyroid hormone secretion, J Clin Endocrinol Metab 92(8) (2007) 3230–8. [PubMed: 17550963]

[5]. Fu L, Patel MS, Bradley A, Wagner EF, Karsenty G, The molecular clock mediates leptin-regulated bone formation, Cell 122(5) (2005) 803–15. [PubMed: 16143109]

[6]. Samsa WE, Vasanji A, Midura RJ, Kondratov RV, Deficiency of circadian clock protein BMAL1 in mice results in a low bone mass phenotype, Bone 84 (2016) 194–203. [PubMed: 26789548]

[7]. Bunger MK, Walisser JA, Sullivan R, Manley PA, Moran SM, Kalscheur VL, Colman RJ, Bradfield CA, Progressive arthropathy in mice with a targeted disruption of the Mop3/Bmal-1 locus, Genesis 41(3) (2005) 122–32. [PubMed: 15739187]

[8]. Storch KF, Paz C, Signorovitch J, Raviola E, Pawlyk B, Li T, Weitz CJ, Intrinsic circadian clock of the mammalian retina: importance for retinal processing of visual information, Cell 130(4) (2007) 730–741. [PubMed: 17719549]

[9]. Logan M, Martin JF, Nagy A, Lobe C, Olson EN, Tabin CJ, Expression of Cre Recombinase in the developing mouse limb bud driven by a Prxl enhancer, Genesis 33(2) (2002) 77–80. [PubMed: 12112875]

[10]. Muzumdar MD, Tasic B, Miyamichi K, Li L, Luo L, A global double-fluorescent Cre reporter mouse, Genesis 45(9) (2007) 593–605. [PubMed: 17868096]

[11]. Nakamura T, Imai Y, Matsumoto T, Sato S, Takeuchi K, Igarashi K, Harada Y, Azuma Y, Krust A, Yamamoto Y, Nishina H, Takeda S, Takayanagi H, Metzger D, Kanno J, Takaoka K, Martin TJ, Chambon P, Kato S, Estrogen prevents bone loss via estrogen receptor alpha and induction of Fas ligand in osteoclasts, Cell 130(5) (2007) 811–23. [PubMed: 17803905]

[12]. Erlebacher A, Derynck R, Increased expression of TGF-beta 2 in osteoblasts results in an osteoporosis-like phenotype, J Cell Biol 132(1-2) (1996) 195–210. [PubMed: 8567723]

[13]. Greenblatt MB, Shim JH, Zou W, Sitara D, Schweitzer M, Hu D, Lotinun S, Sano Y, Baron R, Park JM, Arthur S, Xie M, Schneider MD, Zhai B, Gygi S, Davis R, Glimcher LH, The p38 MAPK pathway is essential for skeletogenesis and bone homeostasis in mice, J Clin Invest 120(7) (2010) 2457–73. [PubMed: 20551513]

[14]. Xu C, Ochi H, Fukuda T, Sato S, Sunamura S, Takarada T, Hinoi E, Okawa A, Takeda S, Circadian Clock Regulates Bone Resorption in Mice, J Bone Miner Res 31(7) (2016) 1344–55. [PubMed: 26841172]

[15]. Takarada T, Xu C, Ochi H, Nakazato R, Yamada D, Nakamura S, Kodama A, Shimba S, Mieda M, Fukasawa K, Ozaki K, Iezaki T, Fujikawa K, Yoneda Y, Numano R, Hida A, Tei H, Takeda S, Hinoi E, Bone Resorption Is Regulated by Circadian Clock in Osteoblasts, J Bone Miner Res 32(4) (2017) 872–881. [PubMed: 27925286]

[16]. Dudek M, Meng QJ, Running on time: the role of circadian clocks in the musculoskeletal system, Biochem J 463(1) (2014) 1–8. [PubMed: 25195734]

[17]. Yu EA, Weaver DR, Disrupting the circadian clock: gene-specific effects on aging, cancer, and other phenotypes, Aging 3(5) (2011) 479–93. [PubMed: 21566258]

[18]. Ermann J, Editorial: Of Mice and Mice: Understanding Conflicting Murine Experimental Data, Arthritis Rheumatol 68(8) (2016) 1801–4. [PubMed: 27059525]

[19]. Joseph F, Ahmad AM, Ul-Haq M, Durham BH, Whittingham P, Fraser WD, Vora JP, Effects of growth hormone administration on bone mineral metabolism, PTH sensitivity and PTH secretory rhythm in postmenopausal women with established osteoporosis, J Bone Miner Res 23(5) (2008) 721–9. [PubMed: 18052753]

[20]. Srivastava AK, Bhattacharyya S, Li X, Mohan S, Baylink DJ, Circadian and longitudinal variation of serum C-telopeptide, osteocalcin, and skeletal alkaline phosphatase in C3H/HeJ mice., Bone 29(4) (2001) 361–7. [PubMed: 11595619]

[21]. Lohstroh PN, Chen J, Ba J, Ryan LM, Xu X, Overstreet JW, Lasley BL, Bone Resorption Is Affected by Follicular Phase Length in Female Rotating Shift Workers, Environmental Health Perspectives 111(4) (2002) 618–622.

[22]. Quevedo I, Zuniga AM, Low bone mineral density in rotating-shift workers, J Clin Densitom 13(4) (2010) 467–9. [PubMed: 21029978]

[23]. Feskanich D, Hankinson SE, Schernhammer ES, Nightshift work and fracture risk: the Nurses' Health Study, Osteoporos Int 20(4) (2009) 537–42. [PubMed: 18766292]

[24]. Rogers TS, Harrison S, Swanson C, Cauley JA, Barrett-Connor E, Orwoll E, Stone KL, Lane NE, G. Osteoporotic Fractures in Men Study Research, Rest-activity circadian rhythms and bone mineral density in elderly men, Bone Rep 7 (2017) 156–163. [PubMed: 29181439]

Highlights

- Bmal1−/− mice with genetic disruption of the circadian molecular clock have a low bone mass phenotype.
- The bone phenotype of Bmal1−/− mice is recapitulated in mice with conditional Bmal1 deletion in mesenchymal cells ($Bmal1^{f/f}$.Prx1-cre), but not in mice with conditional Bmal1 deletion in osteoclasts ($Bmal1^{f/f}$.Ctsk-cre).
- $Bmal1^{f/f}$.Prx1-cre mice exhibit high bone turnover with enhanced bone resorption and bone formation.

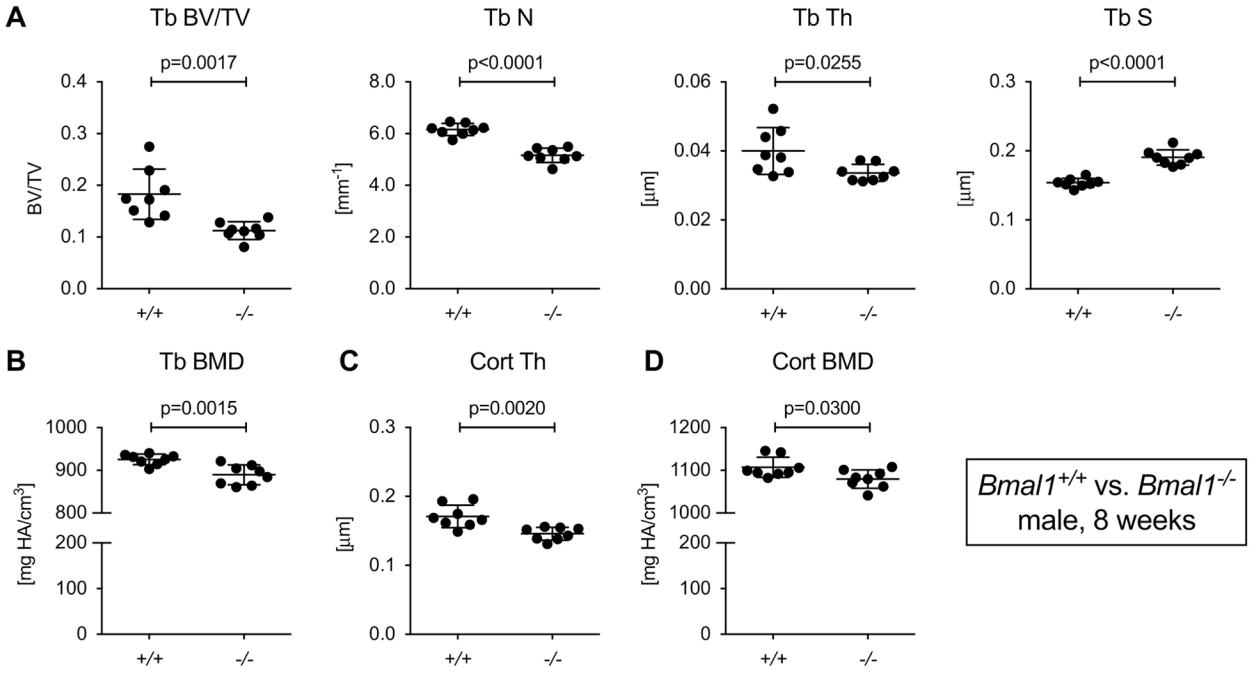

Fig.1. *Bmal1*$^{-/-}$ mice have reduced bone mass.

Femurs from 8-week-old male *Bmal1*$^{+/+}$ and *Bmal1*$^{-/-}$ littermates were analyzed by microCT. (A) Trabecular bone parameters, (B) trabecular BMD, (C) cortical thickness, and (D) cortical BMD. Bars are mean and SD; n=8 animals per group; p values by Student's *t* test. Tb, trabecular; Cort, cortical; BV/TV, bone volume/tissue volume; N, number; Th, thickness; S, separation; BMD, bone mineral density.

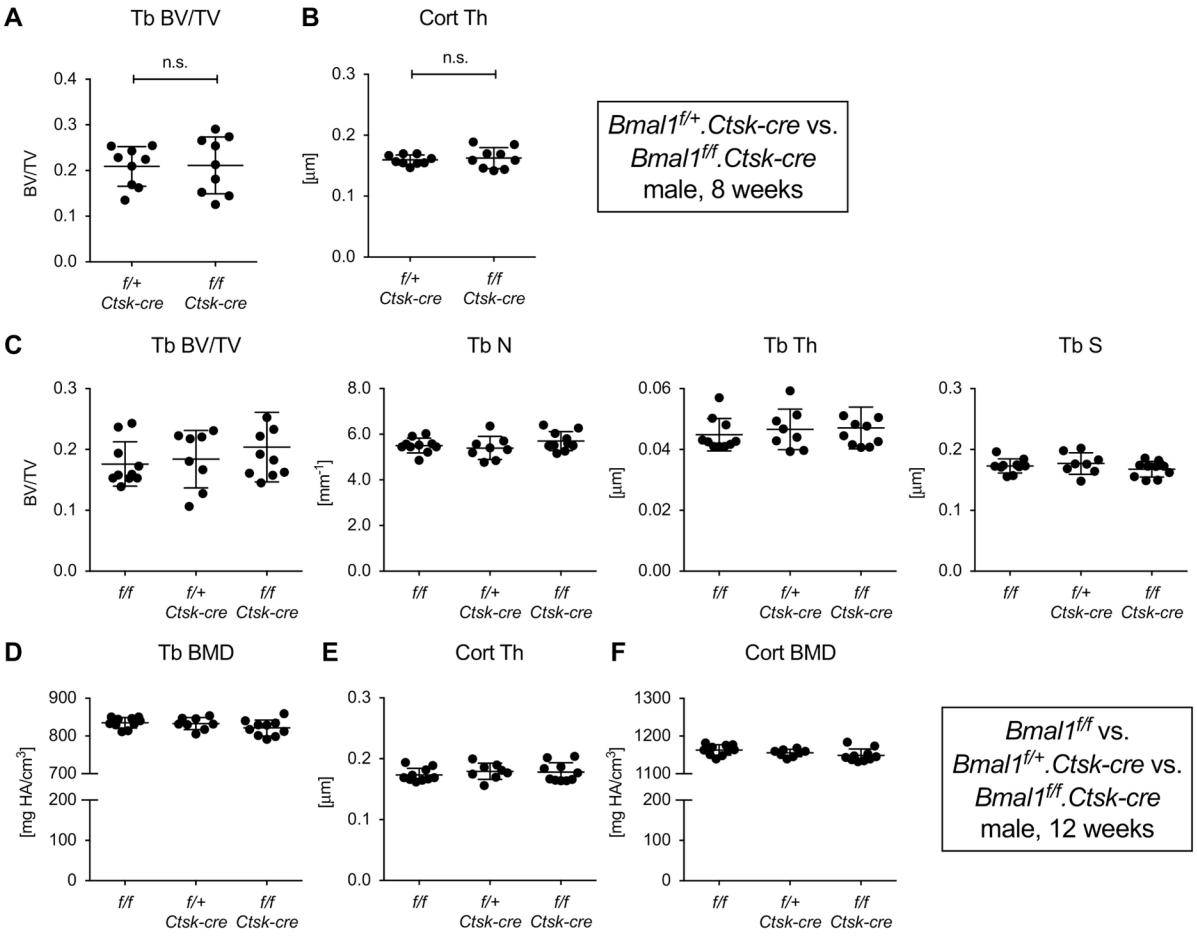

Fig. 2. Mice with conditional deletion of *Bmal1* in osteoclasts lack a bone phenotype.

Femurs from 8-week-old male *Bmal1*$^{f/+}$*.Ctsk-cre* and *Bmal1*$^{f/f}$*.Ctsk-cre* littermates were analyzed by microCT. (A) Trabecular BV/TV, (B) cortical thickness. Subsequently, a three-way analysis of 12-week-old male *Bmal1*$^{f/f}$, *Bmal1*$^{f/+}$·*Ctsk-cre* and *Bmal1*$^{f/f}$*.Ctsk-cre* mice was performed comparing (C) trabecular bone parameters, (D) trabecula BMD, (E) cortical thickness, and (F) cortical BMD. Bars are mean and SD; n=8-10 animals per group. There were no statistically significant differences between groups by Student's *t* test (A, B) or one-way ANOVA (C-F).

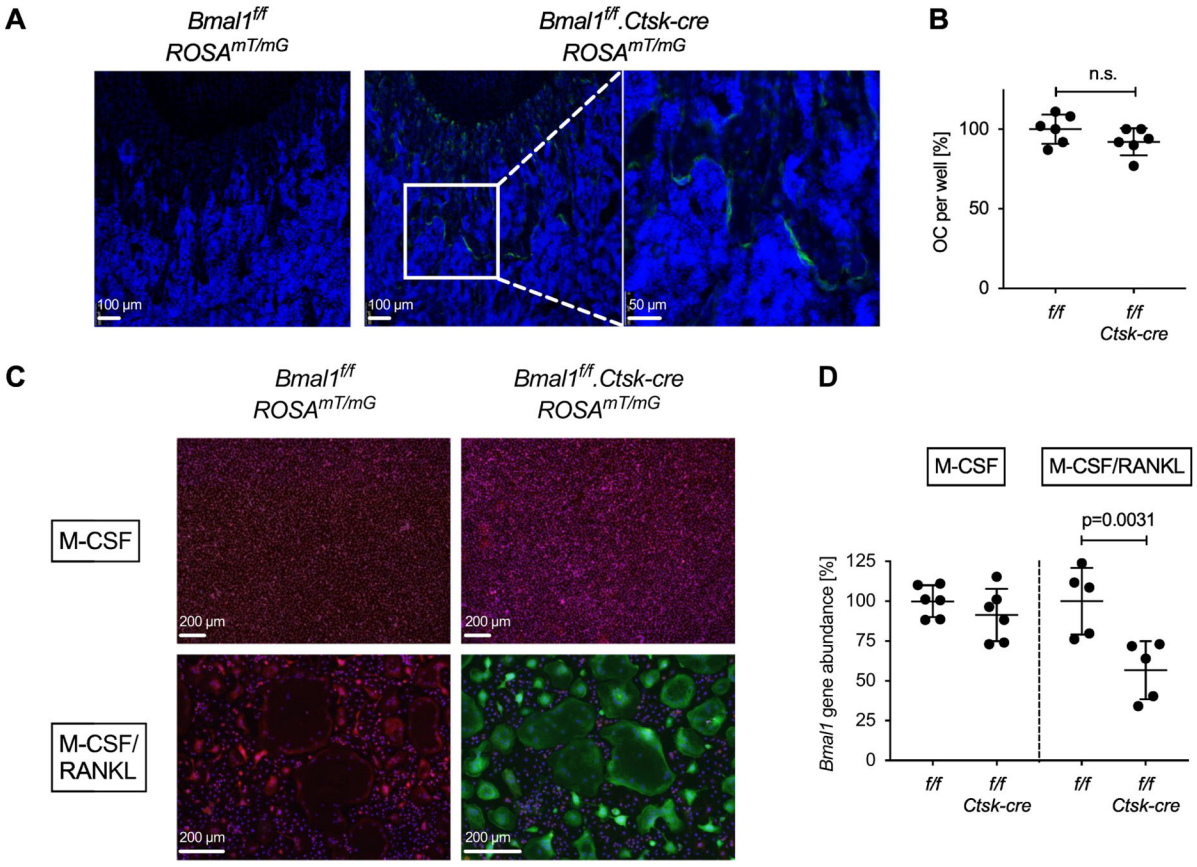

Fig. 3. Deletion of *Bmal1* in osteoclasts from *Bmal1*$^{f/f}$.*Ctsk-cre* mice.

(A) Sections of the distal femur from representative 4-week-old *Bmal1*$^{f/f}$.*ROSA26*$^{mT/mG}$ and *Bmal1*$^{f/f}$.*Ctsk-cre.ROSA26*$^{mT/mG}$ mice analyzed by fluorescence microscopy. Green = EGFP, Blue = DAPI. Positive EGFP fluorescence documents a history of Cre activity. (B) Osteoclasts were differentiated *in vitro* from *Bmal1*$^{f/f}$ and *Bmal1*$^{f/f}$.*Ctsk-cre* bone marrow of individual mice in the presence of M-CSF and RANKL, and the number of TRAP positive osteoclasts per well was counted. Pooled data from two experiments are shown with each symbol representing one animal. Data were normalized to the mean number of *Bmal1*$^{f/f}$ osteoclasts in each experiment (100%). (C) Bone marrow cells from *Bmal1*$^{f/f}$.*ROSA26*$^{mT/mG}$ and *Bmal1*$^{f/f}$.*Ctsk-cre.ROSA26*$^{mT/mG}$ mice were differentiated into osteoclasts as in (B), control macrophages were generated by culture with M-CSF. Green = EGFP, Red = tdTomato. (D) Genomic DNA was prepared from *Bmal1*$^{f/f}$ and *Bmal1*$^{f/f}$.*Ctsk-cre* macrophage (M-CSF) and osteoclast (M-CSF + RANKL) cultures. Deletion of *Bmal1* was assessed by real-time quantitative PCR analysis of genomic DNA. Data were normalized to the *Bmal1* content in macrophage cultures (100%). Each data point represents one animal. Pooled data from two experiments are shown. Bars are mean and SD; p values by Student's *t* test.

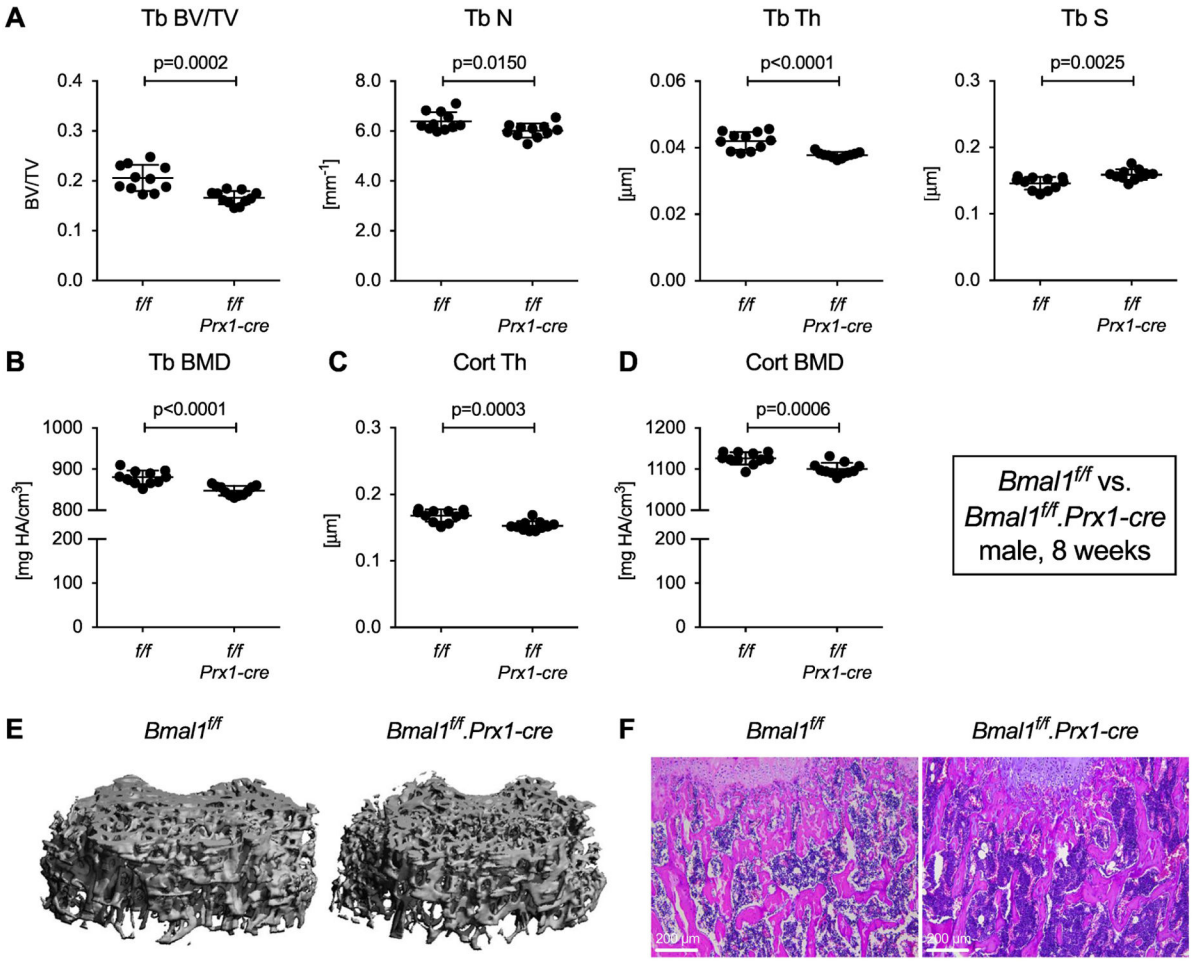

Fig. 4. *Bmal1* deletion in mesenchymal cells reproduces the bone phenotype of *Bmal1* germline knockout mice.

Femurs from 8-week-old male *Bmal1*$^{f/f}$ and *Bmal1*$^{f/f}$.*Prx1-cre* littermates were analyzed by microCT. (A, B) Trabecular bone parameters, (C) cortical thickness, and (D) cortical BMD. Bars are mean and SD; n=10 animals per group; p values by Student's *t* test. (E) 3-D rendering of trabecular bone specimens and (F) representative H&E stained sections of trabecular bone from 8-week-old male *Bmal1*$^{f/f}$ and *Bmal1*$^{f/f}$.*Prx1-cre* mice.

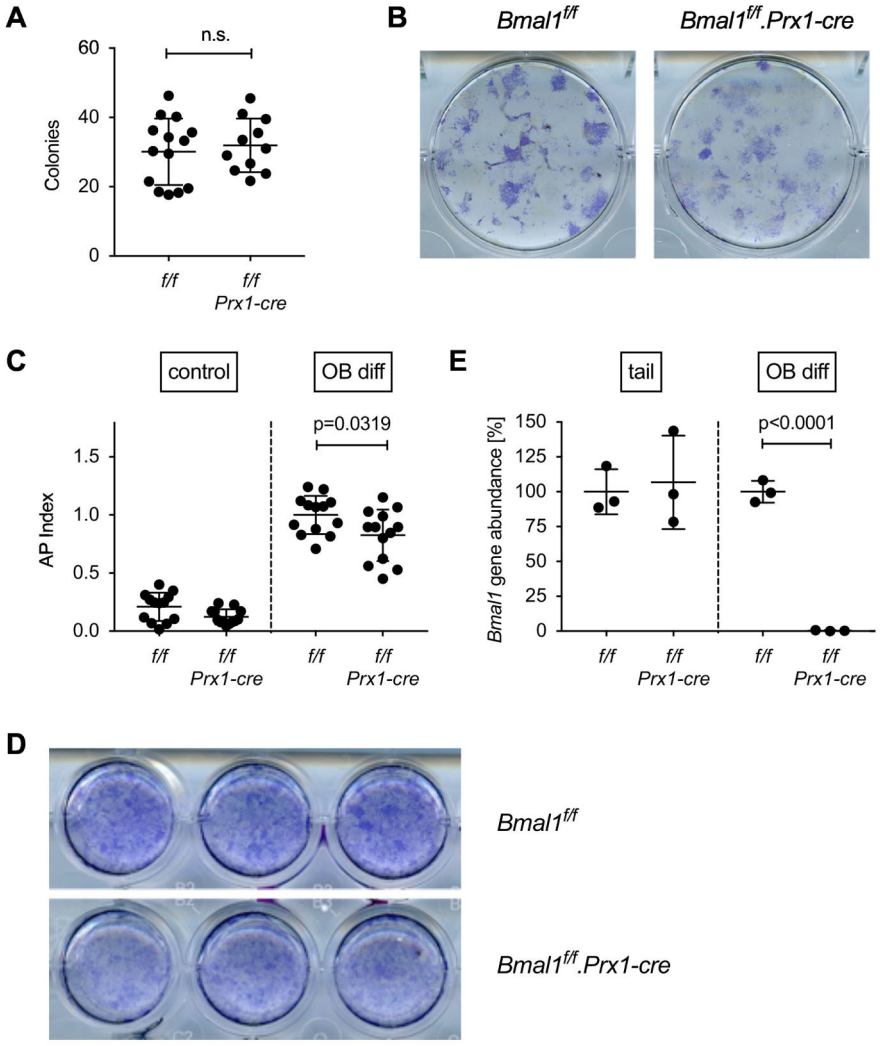

Fig. 5. *In vitro* osteoblast differentiation from *Bmal1*$^{f/f}$*.Prx-cre* bone marrow.

(A) Cells derived by enzymatic digestion of whole long bones from *Bmal1*$^{f/f}$ and *Bmal1*$^{f/f}$*.Prx1-cre* mice were differentiated in osteogenic medium for 21 days, and the number of alkaline phosphatase positive colonies was counted. Each data point represents the mean of triplicate cultures from the bone marrow of one mouse, bars are mean and SD of data pooled from 4 experiments. Representative wells are shown in (B). (C) Osteoblast precursors were differentiated in osteogenic medium for 28 days and assayed for alkaline phosphatase activity using a colorimetric assay. The AP index was calculated by normalizing alkaline phosphatase activity to cell viability measured by Alamar Blue assay. Data points represent the mean of triplicate cultures from the bone marrow of individual mice; bars are mean and SD of data pooled from 4 experiments; p value by Student's *t* test. (D) Representative wells stained with a non-soluble alkaline phosphatase substrate. (E) Genomic DNA isolated from the tail of *Bmal1*$^{f/f}$ and *Bmal1*$^{f/f}$*.Prx1-cre* mice or osteoblast cultures from *Bmal1*$^{f/f}$ and *Bmal1*$^{f/f}$*.Prx1-cre* bone marrow was analyzed for deletion of *Bmal1* by real-time quantitative PCR. Each data point represents one animal; bars are mean and SD; p value by Student's *t* test.

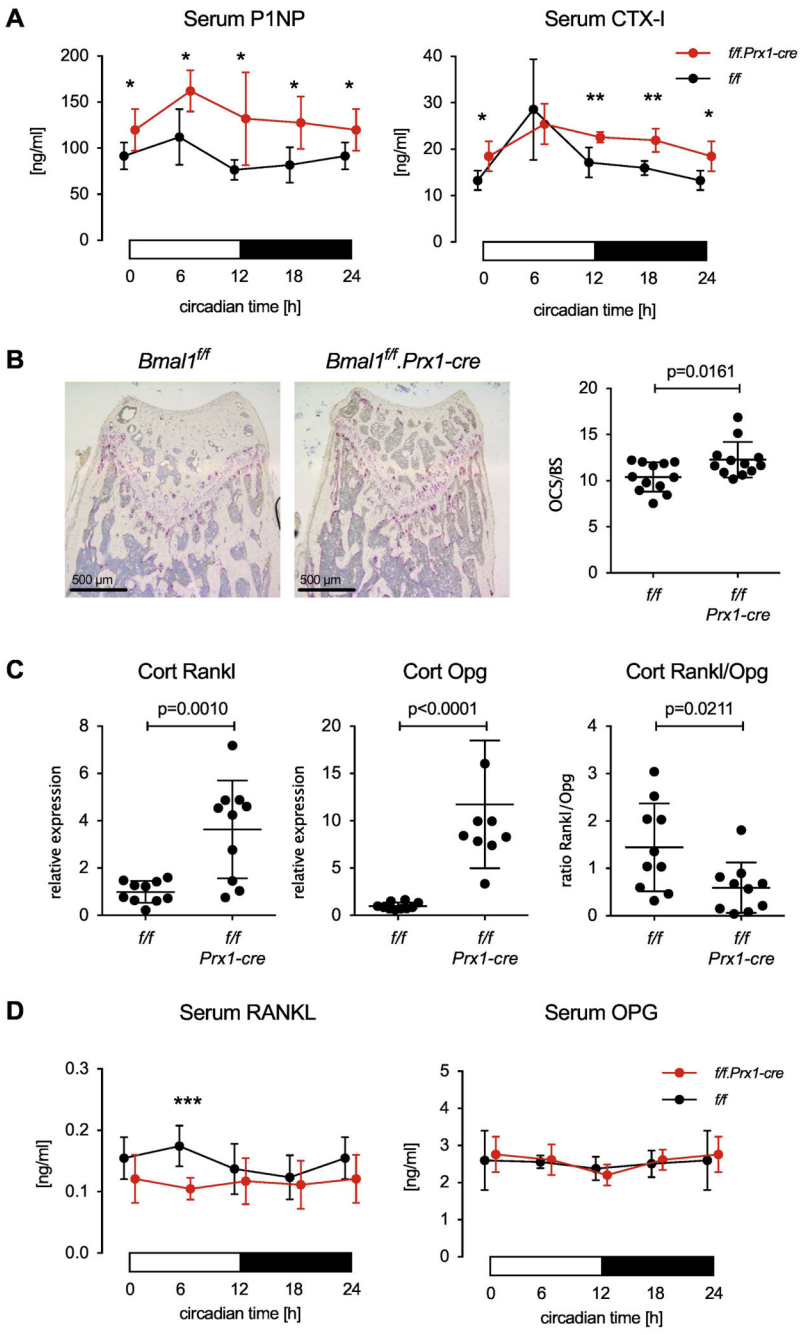

Fig. 6. Enhanced bone turnover in *Bmal1*$^{f/f}$*.Prx-cre* mice.

(A) P1NP and CTX-I measured in the serum of 8-week-old male *Bmal1*$^{f/f}$ and *Bmal1*$^{f/f}$*.Prx1-cre* littermates collected at 6-hour intervals. Data are mean and SD, n=5 animal per time point and genotype, p values by Student's *t* test, * < 0.05, ** < 0.01. (B) Representative TRAP-stained sections of distal femurs from 8-week-old male *Bmal1*$^{f/f}$ and *Bmal1*$^{f/f}$*.Prx1-cre* littermates. Osteoclast surface (OCS) per bone surface (BS) was measured as described in Methods. 2 slides from each of n=6 mice per genotypes were analyzed, bars are mean and SD; p value by Student's *t* test. (C) *Rankl, Opg* and the ratio of *Rankl/Opg* gene expression in cortical bone of 8-week-old male *Bmal1*$^{f/f}$ and *Bmal1*$^{f/f}$*.Prx1-cre*

littermates at circadian time 6h, n=10 animals per genotype, p values by Student's *t* test. (D) RANKL and OPG serum levels in 8-week-old male *Bmal1*$^{f/f}$ and *Bmal1*$^{f/f}$*.Prx1-cre* littermates measured in 6-hour intervals, n=7 animals per time point and genotype, p values by Student's *t* test, *** < 0.001. In (A) and (D), the 0-hour data are shown at both 0 and 24 hours in order to represent a full 24-hour day.